

Ride comfort of the bridge-traffic-wind coupled system considering bridge surface deterioration

Yang Liu¹, Xinfeng Yin^{*1}, Lu Deng² and C.S. Cai³

¹School of Civil Engineering and Architecture, Changsha University of Science & Technology, Changsha 410004, Hunan, China

²College of Civil Engineering, Hunan University, Changsha 410076 Hunan, China

³Department of Civil and Environmental Engineering, Louisiana State University, Baton Rouge, Louisiana 70803, USA

(Received January 3, 2016, Revised May 13, 2016, Accepted May 17, 2016)

Abstract. In the present study, a new methodology is presented to study the ride comfort and bridge responses of a long-span bridge-traffic-wind coupled vibration system considering stochastic characteristics of traffic flow and bridge surface progressive deterioration. A three-dimensional vehicle model with 24 degrees-of-freedom (DOFs) including a three-dimensional non-linear suspension seat model and the longitudinal vibration of the vehicle is firstly presented to study the ride comfort. An improved cellular automaton (CA) model considering the influence of the next-nearest neighbor vehicles and a progressive deterioration model for bridge surface roughness are firstly introduced. Based on the equivalent dynamic vehicle model approach, the bridge-traffic-wind coupled equations are established by combining the equations of motion of both the bridge and vehicles in traffic using the displacement relationship and interaction force relationship at the patch contact. The numerical simulations show that the proposed method can simulate rationally the ride comfort and bridge responses of the bridge-traffic-wind coupled system; and the vertical, lateral, and longitudinal vibrations of the driver seat model can affect significantly the driver's comfort, as expected.

Keywords: bridge; traffic; vibration; ride comfort; bridge surface

1. Introduction

Ride comfort problems of the moving vehicles arise mainly from vibrations of the vehicle body, especially for the vehicles moving on long-span bridges in windy environments. Though the time duration for the vehicle running through a bridge lasts only a few minutes, the short-term ride discomfort could cause seriously the fatigue and affect handling performance of the driver, which may lead to catastrophic vehicle accidents. Thus, the ride comfort has attracted much attention over the past two decades, and some researchers studied the ride comfort by analyzing the vibration of the wind-bridge-vehicle coupled systems (Xu and Guo 2004, Chen and Cai 2004, Yin *et al.* 2011).

To study the wind-bridge-vehicle coupled interaction, some complex vehicle models that can

*Corresponding author, Associate Professor, E-mail: yinxinfeng@163.com

consider the various dynamic properties of vehicles have been developed (Chen and Cai 2004, Law and Zhu 2005, Deng and Cai 2010). Although all these vehicle models do not include the detailed seat model, some of these vehicle models were still used to study the ride comfort for the simplification by ignoring the seat's vibration (Xu and Guo 2004, Yin *et al.* 2011, Cai *et al.* 2015), i.e., the vibration responses of the whole truck body model instead of the seat vibrations were analyzed. This simplification avoids the complexity of simulating the seat model and significantly reduces the computation effort; however, a verification of this simplification needs to be performed before using it with confidence. Thus, in this paper, a three dimensional vehicle model including three-dimensional non-linear suspension seat model is presented to study the ride comfort.

In most existing studies of the wind-bridge-vehicle interaction, researchers either simplified the stochastic traffic flow with multiple vehicles distributed with assumed patterns (Chen and Cai 2007) or modeled the traffic flow as a simplified statistical process (Chen and Feng 2006). For the long-span bridges, such a simplification of the actual vehicle fleet has been found to possibly cause considerable inaccuracy of the predictions for the dynamic performance (Guo and Xu 2001, Chen and Cai 2004). Recently, based on the cellular automaton (CA) traffic flow simulation, Chen and Wu (2010) developed a general bridge dynamic performance analytical model considering the stochastic traffic and wind excitations under normal situations. The effect of the stochastic characteristics on the dynamic performance of long-span bridges is significant (Chen and Wu 2009, 2010, Han 2015, Park 2016). However, those studies were all focused on the dynamic performance of the bridge, but not for the ride comfort, and the used traffic flow model did not take into account the influence of the next-nearest neighbor vehicles, though this influence exists in real traffic and cannot be ignored (Kong *et al.* 2006). The deterioration of the used bridge surface due to vehicle loads or corrosions for the existing bridges was also not considered. In this paper, an improved CA model considering the influence of the next-nearest neighbor vehicles and a progressive deterioration model for bridge-roughness were firstly introduced.

This paper presents a new methodology to study the ride comfort and bridge responses of a long-span bridge-traffic-wind coupled vibration system considering stochastic characteristics of traffic flow and bridge surface progressive deterioration. A three-dimensional vehicle model including a three-dimensional non-linear suspension seat model was presented to study the ride comfort. An improved CA model considering the influence of the next-nearest neighbor vehicles and a progressive deterioration model for bridge-roughness were firstly introduced. The bridge-traffic-wind coupled equations were established by combining the equations of motion of both the bridge and vehicles using the displacement relationship and interaction force relationship at the contact patch. The numerical simulations show that the proposed method can simulate rationally the vibration of the bridge-traffic-wind coupled system, and the vertical, lateral, and longitudinal vibrations of driver seat model can affect significantly the driver's comfort.

2. Method of traffic flow-bridge-wind interaction analysis

2.1 Equations of motion for a three dimensional vehicle-bridge-wind vibration system

In mechanical engineering areas, vehicles are usually modeled in various configurations depending on what is of more concern. In studying the interactions between vehicles and structures, the vehicle model is somewhat simplified to the extent that all the relevant important

information will be included. A review of the different vehicle models used in the literature was reported by Yu and Chan (2007). Most of the vehicle models in vehicle-bridge-wind vibration systems cannot consider the vibration of driver seat model and the longitudinal vibration of the vehicle; however, the vibration of driver seat model and longitudinal vibration of the vehicle may be significant in studying ride comfort.

2.2 Equations of motion of a three-dimensional vehicle model considering the driver seat model

Based on the vehicle model of 12 degrees-of-freedom (DOFs) in Yin *et al.* (2011), in the present study, a new full-scale vehicle model with 24 degrees-of-freedom (DOFs) was developed including a three-dimensional driver seat model and the longitudinal vibration of the vehicle (Figs.1 and 2). The total DOFs include the longitudinal displacements (x_t), vertical displacements (z_t), lateral displacements (y_t), pitching rotations (θ_t), roll displacements (ϕ_t), and yawing angle (φ_t) of the vehicle truck body, and the longitudinal displacement ($x_{al}^1, x_{ar}^1, x_{al}^2$, and x_{ar}^2), vertical displacements ($z_{al}^1, z_{ar}^1, z_{al}^2$, and z_{ar}^2) and lateral displacements ($y_{al}^1, y_{ar}^1, y_{al}^2$, and y_{ar}^2) of the vehicle's first to second axles; and $z_{su}(x_{su}, y_{su})$ and $z_{ss}(x_{ss}, y_{ss})$ represent the vertical(longitudinal, lateral) displacement of the occupant mass m_{su} and suspension seat mass m_{ss} of the driver seat, respectively. In the subscripts, the "t" and "a" represent the truck and axle suspensions, respectively; "l" and "r" represent the left and right on the axles, respectively; and "su" and "ss" represent the occupant mass and suspension seat, respectively.

To simulate the interaction between the vehicle wheel and bridge surface, the wheel was modeled as a three-dimensional elementary spring as shown in Fig. 3, and the mass of the wheel was included in the mass of the axle.

The displacement in the radial direction of the wheel spring (see Fig. 4) at the contact position x can be expressed as:

$$U_{tx} = \{z_a^i + (s/2)\phi_t - [-r_z^i(x)] + \Delta - R(1 - \cos\theta) - z_{bx_contact}^i\} / \cos\theta \quad (1)$$

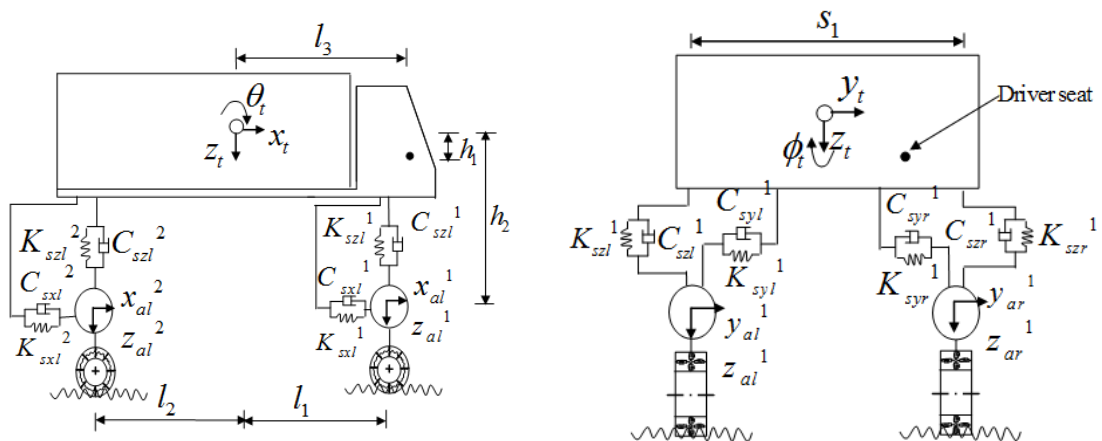


Fig. 1 A new full-scale vehicle model

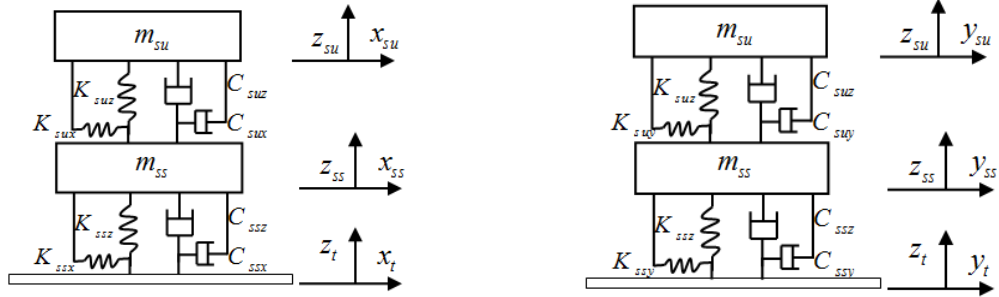


Fig. 2 A three-dimensional driver seat model

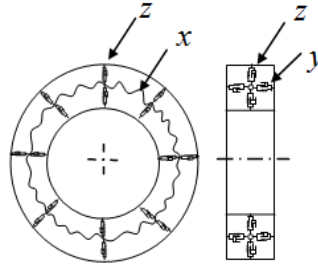


Fig. 3 Schematic diagram of tire model: longitudinal springs (x), lateral springs (y), and radial springs (z)

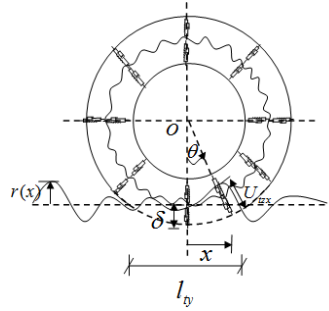


Fig. 4 Schematic diagram of wheel deformation

where U_{tzx} is the vertical deformation of the wheel at the position x ; s is the distance between the right and left wheels; and $\cos \theta = \frac{R - \Delta}{\sqrt{(x)^2 + (R - \Delta)^2}}$. From Eq. (1), one can observe that

U_{tzx} is a function of the vehicle axle displacement z_a^i ; roll displacement of vehicle axle ϕ_t ; wheel radius R ; wheel deformation due to the load of vehicle weight Δ ; and bridge dynamic vertical deflection $z_{bx_contact}^i$ at the contact position x . The $r_z^i(x)$ is the vertical bridge roughness of

the four wheels. The interaction vertical force F_{v-b} acting on the wheel can be obtained as

$$F_{v-b} = -F_{tz} - F_{dtz} \quad (2)$$

Where l_{ty} is the patch length of the wheel; $F_{tz} = \int_{-l_{ty}/2}^{l_{ty}/2} k_{tz} U_{tzx} \cos \theta dx$ is the elastic force due to the vertical deformation of the wheel; $F_{dtz} = \int_{-l_{ty}/2}^{l_{ty}/2} c_{tz} \dot{U}_{tzx} \cos \theta dx$ is the damping force due to the vertical deformation of the wheel; k_{tz} is the spring stiffness per unit length of the wheel in the radial direction; and c_{tz} is the damping coefficient per unit length of the wheel in the radial direction.

According to Gim and Nikravesh (1990), the lateral force of a pneumatic tire-bridge surface interaction can be considered as a resultant force composed of three components of force F_{ys} , $F_{y\alpha}$, and $F_{y\gamma}$ due to the tire running with an ‘‘S’’ shape, slip angle α , and camber angle γ , respectively. The lateral force can be obtained as (See more description and definition in Gim and Nikravesh (1990))

$$F_y = F_{y\alpha} + F_{y\gamma} + F_{ys} \quad (3)$$

$$F_{y\alpha} = -\text{sign}(\alpha) \cdot [C_\alpha S_\alpha l_n^2 + \left(\mu_y - \frac{C_\gamma S_\gamma}{F_{v-b}} \right) F_z (1 - 3l_n^2 + 2l_n^3)] \quad (4a)$$

$$F_{y\gamma} = -\text{sign}(\gamma) \cdot C_\gamma S_\gamma \quad (4b)$$

$$F_{ys} = [k_{ty} (y_a^i + y_{ts} - y_{bx_contact}^i) + c_{ty} (\dot{y}_a^i + \dot{y}_{ts} - \dot{y}_{bx_contact}^i)] l_{tr} \quad (4c)$$

where C_α is the cornering stiffness; S_α is the absolute value of the lateral slip ratio S_{sy} ; a non-dimensional contact patch length l_n is defined as $l_n = l_\alpha / l_{ty}$, where l_α is the length of the adhesion region from the front extremity to the breakaway point for the sliding region of the contact patch, therefore, l_α is varied from 0 to the value of l_{ty} is the patch length of the wheel; μ_y is the tire-bridge surface friction coefficient in the slipping region; F_z is the tire vertical force acting on the bridge surface and equals $-F_{v-b}$; C_γ is the camber stiffness; and S_γ is the absolute value of the lateral slip ratio due to the camber angle γ and defined as: $S_\gamma = |\sin \gamma|$. Based on the studies in Gim and Nikravesh (1990) and Yin *et al.* (2011), the slip angle can be varied from -10° to 10° , and the camber angle varies from -8° to 8° . Furthermore, k_{ty} and c_{ty} are the tire lateral stiffness and damping coefficients per unit length of the wheel; y_a^i is the lateral displacement of the vehicle axle; y_{ts} is the tire lateral displacement due to tire running with an ‘‘S’’ shape; and $y_{bx_contact}^i$ is the bridge dynamic lateral deflection at the contact position x .

The problem of simulating the tire running with an “S” shape is very complex. In this study, to simplify the model, the “S” shape was assumed as a “Sine” shape with a random amplitude and random phase angle, similar to the assumptions made in Fujii and Yoshimoto (1975) and Fujii *et al.* (1975). As a result, y_{ts} can be expressed as

$$y_{ts}(x) = A_s \sin\left(\frac{2\pi x}{l_s} + \varphi_s\right) \quad (5)$$

where A_s is the random amplitude; l_s is the wavelength; and φ_s is the initial phase angle. Based on the studies (Fujii and Yoshimoto 1975, Fujii *et al.* 1975), A_s can be assumed to follow a symmetrical distribution from 2.5 mm to 5 mm; l_s can be obtained from a symmetrical distribution from 6.65 m to 10 m; and φ_s can also be assumed to follow a symmetrical distribution from 0 to 2π .

The longitudinal force of a pneumatic tire-bridge surface interaction can be considered as a resultant force due to the longitudinal deformation and longitudinal friction of the tire. The longitudinal force can be obtained as:

$$F_x = -\text{sign}(S_{sx}) \cdot [C_s S_n l_n^2 + \mu_x F_z (1 - 3l_n^2 + 2l_n^3)] \quad (6)$$

where C_s is the longitudinal stiffness; S_n is the absolute value of the longitudinal slip ratio S_{sx} ; l_n is the non-dimensional contact patch length; μ_x is the tire-bridge surface friction coefficient in the longitudinal (x) direction; and F_z is the tire vertical force acting on the bridge surface equal to $-F_{v-b}$.

$$U_{szl}^1 = z_t - z_{al}^1 + (s_1/2)\phi_t - l_1\theta_t \quad (7)$$

$$U_{s zr}^1 = z_t - z_{ar}^1 - (s_1/2)\phi_t - l_1\theta_t \quad (8)$$

$$U_{szl}^2 = z_t - z_{al}^2 + (s_2/2)\phi_t - l_2\theta_t \quad (9)$$

$$U_{s zr}^2 = z_t - z_{ar}^2 - (s_2/2)\phi_t - l_2\theta_t \quad (10)$$

where l_1 is the distance between the front and the center of the vehicle, l_2 is the distance between the rear axle and the center of the vehicle, s_1 and s_2 are the distance between the right and left mass blocks on the first and second axles, respectively.

The vertical elastic and damping forces of the suspension can be written as

$$F_{szl}^i = K_{szl}^i U_{szl}^i; F_{s zr}^i = K_{s zr}^i U_{s zr}^i \quad (11)$$

$$F_{dszl}^i = C_{szl}^i \dot{U}_{szl}^i; F_{ds zr}^i = C_{s zr}^i \dot{U}_{s zr}^i, i = 1, 2 \quad (12)$$

where K_{szl}^i , $K_{s zr}^i$, and C_{szl}^i , $C_{s zr}^i$ are the suspension spring stiffness and damping of the i th axle, respectively.

The lateral and longitudinal displacements of the suspension springs can be written as

$$U_{syl}^1 = y_t - y_{al}^1 - l_1\varphi_t + h_1\phi_t, U_{s yr}^1 = y_t - y_{ar}^1 - l_1\varphi_t - h_1\phi_t \quad (13a)$$

$$U_{syl}^2 = y_t - y_{al}^2 + l_2\phi_t + h_1\phi_t; U_{syr}^2 = y_t - y_{ar}^2 + l_2\phi_t - h_1\phi_t \quad (13b)$$

$$U_{sxl}^i = x_t - x_{al}^i; U_{sxr}^i = x_t - x_{ar}^i, i = 1, 2 \quad (13c)$$

where h_l is the height of the vehicle center to the driver seat.

The lateral and longitudinal elastic and damping forces of the suspension can be written as

$$F_{syl}^i = K_{syl}^i \cdot U_{syl}^i; F_{dsyl}^i = C_{syl}^i \cdot \dot{U}_{syl}^i; F_{syr}^i = K_{syr}^i \cdot U_{syr}^i; F_{dsyr}^i = C_{syr}^i \cdot \dot{U}_{syr}^i \quad (14a)$$

$$F_{sxl}^i = K_{sxl}^i \cdot U_{sxl}^i; F_{dsxl}^i = C_{sxl}^i \cdot \dot{U}_{sxl}^i; F_{sxl}^i = K_{sxl}^i \cdot U_{sxl}^i; F_{dsxr}^i = C_{sxr}^i \cdot \dot{U}_{sxr}^i; i = 1, 2 \quad (14b)$$

The equations of motion of the full-scale vehicle can be obtained from the Lagrangian formulation, and can be written as

$$m_t \ddot{x}_t + F_{sxl}^1 + F_{sxr}^1 + F_{sxl}^2 + F_{sxr}^2 + F_{dsxl}^1 + F_{dsxr}^1 + F_{dsxl}^2 + F_{dsxr}^2 = F_{xw} \quad (15a)$$

$$m_t \ddot{y}_t + F_{syl}^1 + F_{syr}^1 + F_{syl}^2 + F_{syr}^2 + F_{dsyl}^1 + F_{dsyr}^1 + F_{dsyl}^2 + F_{dsyr}^2 = F_{yw} \quad (15b)$$

$$m_t \ddot{z}_t + F_{szl}^1 + F_{s zr}^1 + F_{szl}^2 + F_{s zr}^2 + F_{dszl}^1 + F_{ds zr}^1 + F_{dszl}^2 + F_{ds zr}^2 = m_t g + F_{zw} \quad (15c)$$

$$I_{xt} \ddot{\phi}_t + (s_1 / 2)(F_{szl}^1 - F_{s zr}^1) + (s_2 / 2)(F_{szl}^2 - F_{s zr}^2) + \quad (15d)$$

$$(s_1 / 2)(F_{dszl}^1 - F_{ds zr}^1) + (s_2 / 2)(F_{dszl}^2 - F_{ds zr}^2) = M_{xw}$$

$$I_{yt} \ddot{\phi}_t + l_1(F_{syl}^1 + F_{syr}^1) - l_2(F_{syl}^2 + F_{syr}^2) + l_1(F_{dsyl}^1 + F_{dsyr}^1) - l_2(F_{dsyl}^2 + F_{dsyr}^2) = M_{yw} \quad (15e)$$

$$I_{zt} \ddot{\theta}_t + l_1(F_{szl}^1 + F_{s zr}^1) - l_2(F_{szl}^2 + F_{s zr}^2) + l_1(F_{dszl}^1 + F_{ds zr}^1) - l_2(F_{dszl}^2 + F_{ds zr}^2) = M_{zw} \quad (15f)$$

$$m_{al}^i \ddot{x}_{al}^i - F_{dsxl}^i - F_{sxl}^i + F_{xl}^i = 0; m_{ar}^i \ddot{x}_{ar}^i - F_{dsxr}^i - F_{sxr}^i + F_{xr}^i = 0 \quad i = 1, 2 \quad (15g)$$

$$m_{al}^i \ddot{y}_{al}^i - F_{dsyl}^i - F_{syl}^i + F_{yl}^i = 0; m_{ar}^i \ddot{y}_{ar}^i - F_{dsyr}^i - F_{syr}^i + F_{yr}^i = 0 \quad i = 1, 2 \quad (15h)$$

$$m_{al}^i \ddot{z}_{al}^i - F_{szl}^i + F_{t zl}^i - F_{dszl}^i + F_{dtzl}^i = m_{al}^i g \quad i = 1, 2 \quad (15i)$$

$$m_{ar}^i \ddot{z}_{ar}^i - F_{s zr}^i + F_{t zr}^i - F_{ds zr}^i + F_{dt zr}^i = m_{ar}^i g \quad i = 1, 2 \quad (15j)$$

where m_t , m_{al}^i , m_{ar}^i represent the mass of the vehicle body and the i th axle, respectively.

A six-DOF three-dimensional driver seat model, as shown in Fig. 2, is used to study the vibration of the driver seat (Bouazara *et al.* 2006), and the equations of the motion for the suspension seat are given

$$m_{su} \ddot{x}_{su} = K_{sux} (x_{su} - x_{ss}) + C_{sux} (\dot{x}_{su} - \dot{x}_{ss}) \quad (16a)$$

$$m_{su} \ddot{y}_{su} = K_{suy} (y_{su} - y_{ss}) + C_{suy} (\dot{y}_{su} - \dot{y}_{ss}) \quad (16b)$$

$$m_{su} \ddot{z}_{su} = m_{su} g - K_{suz} (z_{su} - z_{ss}) - C_{suz} (\dot{z}_{su} - \dot{z}_{ss}) \quad (16c)$$

$$m_{ss} \ddot{x}_{ss} = K_{sux}(x_{su} - x_{ss}) + C_{sux}(\dot{x}_{su} - \dot{x}_{ss}) - K_{ssx}(x_{ss} - x_t) - C_{ssx}(\dot{x}_{ss} - \dot{x}_t) \quad (16d)$$

$$m_{ss} \ddot{y}_{ss} = K_{suy}(y_{su} - y_{ss}) + C_{suy}(\dot{y}_{su} - \dot{y}_{ss}) - K_{ssy}(y_{ss} - y_t) - C_{ssy}(\dot{y}_{ss} - \dot{y}_t) \quad (16e)$$

$$m_{ss} \ddot{z}_{ss} = m_{ss} g + K_{suz}(z_{su} - z_{ss}) + C_{suz}(\dot{z}_{su} - \dot{z}_{ss}) - K_{ssz}(z_{ss} - z_t) - C_{ssz}(\dot{z}_{ss} - \dot{z}_t) \quad (16f)$$

where $z_{su}(x_{su}, y_{su})$ and $z_{ss}(x_{ss}, y_{ss})$ represent the vertical (longitudinal, lateral) displacement of the occupant mass m_{su} and suspension seat mass m_{ss} , respectively. $K_{sux}(K_{suy}, K_{suz})$ and $C_{sux}(C_{suy}, C_{suz})$ represent the vertical(longitudinal, lateral) stiffness and damping of the occupant mass m_{su} and suspension seat mass m_{ss} , respectively.

Eqs. (15(a))-(16(f)) can be rewritten in a matrix form as

$$[M_v]\{\ddot{U}_v\} + [C_v]\{\dot{U}_v\} + [K_v]\{U_v\} = \{F_G\} + \{F_{v-b}\} + \{F_{vw}\} \quad (17)$$

where $[M_v]$, $[C_v]$, and $[K_v]$ = the mass, damping, and stiffness matrices of the vehicle, respectively; $\{U_v\}$ = the vector including the displacements of the vehicle; $\{F_G\}$ = gravity force vector of the vehicle; $\{F_{v-b}\}$ = vector of the wheel-bridge contact forces acting on the vehicle; and $\{F_{vw}\}$ = vector of the wind forces acting on the vehicle.

2.3 Simplified quasi-steady wind forces on a three-dimensional vehicle model

Wind action on a running vehicle includes static and dynamic load effects. The quasi static wind forces on vehicles are adopted (Baker 1991, Chen and Cai 2004)

$$\begin{aligned} F_{xw} &= \frac{1}{2} \rho_\alpha A U_R^2 C_D(\psi); & F_{zw} &= \frac{1}{2} \rho_\alpha A U_R^2 C_L(\psi); & F_{yw} &= \frac{1}{2} \rho_\alpha A U_R^2 C_S(\psi); \\ M_{xw} &= \frac{1}{2} \rho_\alpha A h_v U_R^2 C_R(\psi); & M_{yw} &= \frac{1}{2} \rho_\alpha A h_v U_R^2 C_P(\psi); & M_{zw} &= \frac{1}{2} \rho_\alpha A h_v U_R^2 C_Y(\psi) \end{aligned} \quad (18)$$

where F_{xw} , F_{yw} , F_{zw} , M_{xw} , M_{yw} and M_{zw} are the drag force, side force, lift force, rolling moment, pitching moment and yawing moment acting on the vehicle, respectively. ρ_α is the air density. C_D , C_S , C_L , C_R , C_P and C_Y are the coefficients of drag force, side force, lift force, rolling moment, pitching moment and yawing moment for the vehicle, respectively. "A" is the frontal area of the vehicle; h_v is the distance from the gravity center of the vehicle to the bridge surface; and U_R is the relative wind speed to the vehicle, which is defined as

$$U_R^2 = [(U + u(x,t)) \cos \beta + \dot{S}]^2 + [(U + u(x,t)) \sin \beta]^2 \quad (19)$$

$$\tan \psi = \frac{(U + u(x,t)) \sin \beta}{(U + u(x,t)) \cos \beta + \dot{S}}$$

where \dot{S} is the driving speed of vehicle; U and $u(x, t)$ are the mean wind speed and turbulent wind speed component on the vehicle, respectively; β is the attack angle of the wind to the vehicle, which is the angle between the wind direction and the vehicle moving direction; and ψ is usually between 0 to π .

2.4 Wind forces on bridge in modal coordinates

The dynamic model of long-span bridges can be obtained through finite element method using different kinds of finite elements such as beam elements and truss elements. With the obtained mode shapes, the response corresponding to any point along the bridge deck can be evaluated in the time domain. The structural nonlinearity is typically considered in the static analysis before a dynamic analysis is conducted. Equations of motions in the three directions including vertical, lateral, and torsion of the bridge with the mode superposition technique can be obtained and can be rewritten in a matrix form as (Clough and Penzien 1993, Chen and Cai 2004)

$$[M_b]\{\ddot{U}_b\} + [C_b]\{\dot{U}_b\} + [K_b]\{U_b\} = \{F_{bw}\} \quad (20)$$

where $[M_b]$, $[C_b]$, and $[K_b]$ are the mass, damping, and stiffness matrices of the bridge, respectively; $\{U_b\}$ is the displacement vector for all DOFs of the bridge; $\{\dot{U}_b\}$ and $\{\ddot{U}_b\}$ are the first and second derivative of $\{U_b\}$ with respect to time, respectively; and $\{F_{bw}\}$ is the vector of the wind forces acting on the bridge.

2.5 Assembling the vehicle-bridge-wind coupled system

Using the displacement relationship and interaction force relationship at the contact patches, the vehicle-bridge coupled system can be established by combining the equations of motion of both the bridge and vehicles (Yin *et al.* 2011), as shown below

$$\begin{aligned} & \begin{Bmatrix} [M_b] \\ [M_v^N] \end{Bmatrix} \begin{Bmatrix} \ddot{U}_b \\ \ddot{U}_v^N \end{Bmatrix} + \begin{Bmatrix} [C_b] + [C_{b-vb}^N] & [C_{b-v}^N] \\ [C_{v-b}^N] & [C_v^N] + [C_{v-v}^N] \end{Bmatrix} \begin{Bmatrix} \dot{U}_b \\ \dot{U}_v^N \end{Bmatrix} + \\ & \begin{Bmatrix} [K_b] + [K_{b-vb}^N] & [K_{b-v}^N] \\ [K_{v-b}^N] & [K_v^N] + [K_{v-v}^N] \end{Bmatrix} \begin{Bmatrix} U_b \\ U_v^N \end{Bmatrix} = \begin{Bmatrix} [F_{b-v}^N] + [F_{vw}^N] \\ [F_{v-b}^N] + [F_G^N] + [F_{bw}^N] \end{Bmatrix} \end{aligned} \quad (21)$$

where N is the number of vehicles traveling on the bridge, $[M_v^N]$, $[C_v^N]$, and $[K_v^N]$ are mass, damping, and stiffness matrices for the traffic, respectively; $[C_{b-vb}^N]$ and $[K_{b-vb}^N]$ are damping and stiffness contribution to the bridge structure due to the coupling effects between the N vehicles in the traffic flow and the bridge system, respectively; $[C_{b-v}^N]$ and $[K_{b-v}^N]$ are the coupled stiffness and damping matrices contributing to bridge vibration from the N vehicles in the traffic flow, respectively; $[C_{v-b}^N]$ and $[K_{v-b}^N]$ are the coupled damping and stiffness matrices contributing to the vibration of the N vehicles, respectively; $[C_{v-v}^N]$ and $[K_{v-v}^N]$ are the coupled damping and stiffness matrices of induced by other vehicles in the traffic flow, respectively. When the vehicle is moving across the bridge, the vehicle-bridge-wind contact points change with the vehicle position and the road-roughness at the contact point. As a large number of degrees of freedom (DOF) are involved, the bridge mode superposition technique is used to simplify the modeling procedure based on the obtained bridge mode shape $\{\Phi_i\}$ and the corresponding natural

circular frequencies ω_i . Bridge performance is practically in the linear range, which justifies the use of the modal superposition approach. Consequently, the number of equations in Eq. (21) and the complexity of the whole procedure are greatly reduced. Eq. (21) can be solved by the *Newmark* method in the time domain.

3. Equations of motion for traffic flow-bridge-wind vibration system

3.1 Traffic flow simulation results considering the influence of the next-nearest neighbor vehicles

The traffic simulation using the CA traffic model can capture the basic features of the probabilistic traffic flow by adopting the realistic traffic rules such as car-following and lane-changing, as well as actual speed limits. One of the most important CA models is NaSch model (Nagel and Schreckenberg 1992). Though NaSch model is simple, it can describe some traffic phenomena in reality, such as phase transition etc. In recent years, the CA traffic model was introduced and verified to study the vibration of bridges under the traffic flow (Chen and Wu 2010). However, all those aforementioned CA models above do not take into account the influence of the next-nearest neighbor vehicles, though this influence exists in real traffic and cannot be ignored (Kong *et al.* 2006). In this paper, an improved CA model considering the influence of the next-nearest neighbor vehicles in Kong *et al.* (2006) is introduced and used to simulate the traffic flow.

In the car-following model, most researchers usually consider the influence of the vehicle ahead using the following equation (Kong *et al.* 2006)

$$\ddot{x}_n(t+T) = \lambda(\dot{x}_{n+1} - \dot{x}_n) \quad (22)$$

where T is a response time lag, λ is the sensitivity coefficient, \ddot{x}_n is the acceleration of the n th vehicle, and \dot{x}_n is the velocity of the n th vehicle, \dot{x}_{n+1} is the velocity of the $(n+1)$ th vehicle.

The model shows that the response of the following vehicle is in direct proportion to the stimulus received from the leading vehicle. Considering the influence of the next-nearest neighbor vehicles, the Eq. (22) can be changed to

$$\ddot{x}_n = \lambda_1(\dot{x}_{n+1} - \dot{x}_n)_{t-T_1} + \lambda_2(\dot{x}_{n+2} - \dot{x}_n)_{t-T_2} \quad (23)$$

where T_1 is a response time lag of the nearest neighbor ahead, T_2 is a response time lag of the next-nearest neighbor ahead, λ_1 and λ_2 are the sensitivity coefficients of the nearest neighbor and next nearest neighbor vehicles, respectively, and both of them are confined between 0 and 1.

Driving strategies are based on the double-look-ahead model for the acceleration step in the NaSch model. According to Eq. (23), suppose $\lambda_1 > \lambda_2$, the acceleration of the vehicle is written as

$$\ddot{x}_n(t+1) = \tilde{\lambda}(\Delta\dot{x}_{n+1}(t), \Delta\dot{x}_{n+2}(t-1)) \quad (24)$$

where $\tilde{\lambda} = \lambda_1(\dot{x}_{n+1}(t) - \dot{x}_n(t)) + \lambda_2(\dot{x}_{n+2}(t-1) - \dot{x}_n(t-1))$. Using Eq. (24), the rule of the acceleration /deceleration can be changed in the NaSch model.

3.2 Equivalent dynamic vehicle model approach

As discussed by Chen and Cai (2007), the vehicle-bridge-wind coupled Eq. (21) can consider various types and numbers of vehicles at any location on the bridge. When the real traffic flow is simulated, the dynamic model of each vehicle will be substituted into Eq. (21) for a “fully coupled” Bridge-Traffic-Wind dynamic interaction analysis. In order to simplify the vehicular models in traffic, all the vehicles are classified as three types: (1) v1-heavy multi-axle trucks; (2) v2-light trucks and buses; and (3) v3-sedan car. Only heavy trucks are modeled with 24 DOFs of the three dimensional vehicle models, light trucks and sedan cars are used with the single DOF of vehicle model to be computationally efficient. The 24 DOFs and single DOF vehicle models are shown in Figs. 1 and 5, respectively. Mechanical and geometric properties are listed in Tables 1 and 2 and can be obtained from Yin *et al.* (2011) and Chen and Cai (2007).

Table 1 The parameters of the three dimensional vehicle with 24 DOFs

Truck Parameter	Value
Mass of truck body m_t	26745 kg
Pitching moment of inertia of truck body I_{zt}	172,160 kg.m ²
Rolling moment of inertia of truck body I_{xt}, I_{yt}	61,496 kg.m ²
Mass of truck front axle m_{a1}, m_{a2}	710kg
Mass of truck rear axle m_{a3}, m_{a4}	800kg
Suspension spring vertical stiffness of the first axle K_{sz}^1, K_{sz}^2	242604 (N/m)
Suspension spring longitudinal/lateral stiffness of the first axle $K_{sy}^1, K_{sy}^2, K_{sx}^1, K_{sx}^2$	102302 (N/m)
Suspension vertical damper of the first axle C_{sz}^1, C_{sz}^2	2190 (N.s/m)
Suspension longitudinal/lateral damper of the first axle $C_{sy}^1, C_{sy}^2, C_{sx}^1, C_{sx}^2$	1690(N.s/m)
Suspension spring vertical stiffness of the second axle K_{sz}^3, K_{sz}^4	1903172(N/m)
Suspension spring longitudinal/lateral stiffness of the second axle $K_{sy}^3, K_{sy}^4, K_{sx}^3, K_{sx}^4$	1003031(N/m)
Suspension vertical damper of the second axle C_{sz}^3, C_{sz}^4	7882(N.s/m)
Suspension longitudinal/lateral damper of the second axle $C_{sy}^3, C_{sy}^4, C_{sx}^3, C_{sx}^4$	5869(N.s/m)
Radial direction spring stiffness of the tire k_{ty}	276770 (N/m)
Radial direction spring damper coefficient of the tire c_{ty}	1990 (N.s/m)
Length of the patch contact	345 mm
Width of the patch contact	240 mm
Distance between the front and the center of the truck l_1	3.73 m
Distance between the rear axle and the center of the truck l_2	1.12 m
Distance between the right and left axles s_l	2.40 m
Occupant mass m_{su}	80 kg
Suspension seat mass m_{ss}	10 kg
Vertical stiffness of the occupant mass K_{suz}	67500(N/m)
Longitudinal or lateral stiffness of the occupant mass K_{sux}, K_{suy}	33750(N/m)
Vertical damping of the occupant mass C_{suz}	528(N.s/m)
Longitudinal/lateral damping of the occupant mass C_{sux}, C_{suy}	321(N.s/m)
Vertical stiffness of the suspension seat mass K_{ssz}	67400(N/m)
Longitudinal or lateral stiffness of the suspension seat mass K_{ssx}, K_{ssy}	33700(N/m)
Vertical damping of the suspension seat mass C_{ssz}	734(N.s/m)
Longitudinal/lateral damping of the suspension seat mass C_{ssx}, C_{ssy}	421(N.s/m)

Table 2 The parameters of the single DOF vehicle model

Parameters	unit	Sedan car	Light truck
Sprung mass	kg	1611	4870
Stiffness of suspension system($K_{sx}^I, K_{sy}^I, K_{sz}^I$)	N/m	434920	500000
Damping($C_{sx}^I, C_{sy}^I, C_{sz}^I$)	N.s/m	5820	20000



Fig. 5 The single DOF vehicle model with three dimensional vibrations

3.3 Modeling of progressive deterioration for bridge surface

The bridge surface profile is assumed usually to be a zero-mean stationary Gaussian random process and can be generated through an inverse Fourier transformation based on a power spectral density (PSD) function (Yin *et al.* 2011) as

$$r^i(x) = \sum_{k=1}^N \sqrt{2\varphi(n_k)\Delta n} \cos(2\pi n_k x + \theta_k) \quad (25)$$

where θ_k is the random phase angle uniformly distributed from 0 to 2π ; $\varphi()$ is the PSD function (m^3/cycle) for the bridge surface elevation; and n_k is the spatial frequency (cycle/m). In the present study, the following PSD function (Yin *et al.* 2011) was used

$$\varphi(n) = \varphi(n_0) \left(\frac{n}{n_0}\right)^{-2} \quad (n_1 < n < n_2) \quad (26)$$

where n is the spatial frequency (cycle/m); n_0 is the discontinuity frequency of $1/2\pi$ (cycle/m); $\varphi(n_0)$ is the roughness coefficient (m^3/cycle) whose value is chosen depending on the bridge condition; and n_1 and n_2 are the lower and upper cut-off frequencies, respectively. The International Organization for Standardization (ISO) (1995) has proposed a bridge roughness classification index from A (very good) to H (very poor) according to different values of $\varphi(n_0)$.

In order to consider the bridge surface damages due to loads or corrosions, a progressive deterioration model for bridge roughness is necessary. To study the fatigue reliability assessment for existing bridges considering bridge surface conditions, the progressive deterioration model of

bridge roughness changing with time was obtained in Zhang and Cai (2012) and can be used in the following

$$\begin{aligned} \varphi(n_0)_t = & 6.1972 \times 10^{-9} \times \exp\{[1.04e^{\eta t} \cdot IRI_0 + \\ & 263(1 + \text{SNC})^{-5}(\text{CESAL})_t] / 0.42808\} + 2 \times 10^{-6} \end{aligned} \quad (27)$$

where IRI_0 is the initial roughness value directly after completing the construction, t is the time in years, and η is the environmental coefficient varying from 0.01 to 0.7 that depends on dry or wet, freezing or nonfreezing conditions. SNC is a parameter that is calculated from data on the strength and thickness of each layer in the pavement, and $(\text{CESAL})_t$ is the estimated number of traffic in terms of AASHTO 80-kN (18-kip) cumulative equivalent single axle load at time t in millions.

Using Eq. (24), the calculated results in Zhang and Cai (2012) are shown in Tables 3 and 4. For the slow lane the bridge condition in the first 8 years was classified as very good, the ninth and tenth years as good, the eleven and twelfth years as average, the thirteen year as poor, and the fourteenth and fifteenth years as very poor. Therefore, the suitable time of repairing bridge surface roughness may be between the 8th to 10th years for the bridge.

3.4 The method of evaluating ride comfort

The ISO2631-1(1997) specifies the root-mean-square (RMS) magnitudes of the vibration acceleration as the standard for ride comfort as shown in Table 5.

Table 3 The variation of road condition for slow lane in 15 years

Years	Roughness coefficient $\varphi(n_0)$	Roughness classification
$1 \leq t \leq 8$	5×10^{-6}	Very good
$9 \leq t \leq 10$	20×10^{-6}	Good
$11 \leq t \leq 12$	80×10^{-6}	Average
$t = 13$	320×10^{-6}	Poor
$14 \leq t \leq 15$	1280×10^{-6}	Very poor

Table 4 The variation of road condition for fast lane in 15 years

Years	Roughness coefficient $\varphi(n_0)$	Roughness classification
$1 \leq t \leq 10$	5×10^{-6}	Very good
$11 \leq t \leq 12$	20×10^{-6}	Good
$t = 13$	80×10^{-6}	Average
$14 \leq t \leq 15$	320×10^{-6}	Poor

Table 5 Ride comfort standard specified in ISO2631-1

Vibration acceleration magnitudes a_w	Comfort or Discomfort
Less than 0.315m/s ²	Not uncomfortable
0.315m/s ² to 0.63 m/s ²	A little uncomfortable
0.5 m/s ² to1 m/s ²	Fairly uncomfortable
0.8 m/s ² to1.6 m/s ²	Uncomfortable
1.25 m/s ² to2.5 m/s ²	Very uncomfortable
Greater than 2 m/s ²	Extremely uncomfortable

For vibrations in more than one direction, the weighted RMS acceleration a_w determined from the vibrations in the orthogonal coordinates is calculated as

$$a_w = (k_{ax}^2 a_{wx}^2 + k_{ay}^2 a_{wy}^2 + k_{az}^2 a_{wz}^2)^{\frac{1}{2}} \quad (28)$$

where a_w is the weighted RMS acceleration; a_{wx} , a_{wy} , and a_{wz} are the weighted RMS accelerations with respect to the orthogonal axes x , y , and z , respectively; k_{ax} , k_{ay} , and k_{az} are multiplying factors with the orthogonal axes x , y , and z , respectively and

$$a_{wj} \Big|_{j=x,y,z} = \left[\frac{1}{T} \int_{t=0}^{t=T} a_{wj}^2(t) \Big|_{j=x,y,z} dt \right]^{\frac{1}{2}} \quad (29)$$

where $a_{wj}(t) \Big|_{j=x,y,z}$ is the acceleration as a function of time (m/s²) in the x , y , and z axle directions; and T is the duration of the measurement (s).

From the relationship of the weighted RMS accelerations a_w and the comfort standard, it can be seen that, in addition to the vertical accelerations, the lateral and longitudinal accelerations of the driver seat will also affect the ride comfort.

4. Numerical studies

4.1 Description of the cable-stayed bridge

As a prototype bridge used in the present study, the Jinyu Highway Bridge, located at the border of Hunan province in China, is an unsymmetrical hybrid cable-stayed bridge with a box section, double towers, double cable planes, and with spans of 80 m+208 m+716 m+70 m+2x65 m from the north to the south, as shown in Fig. 6. A numerical model was created using the FE method with ANSYS software, as seen in Fig. 7.

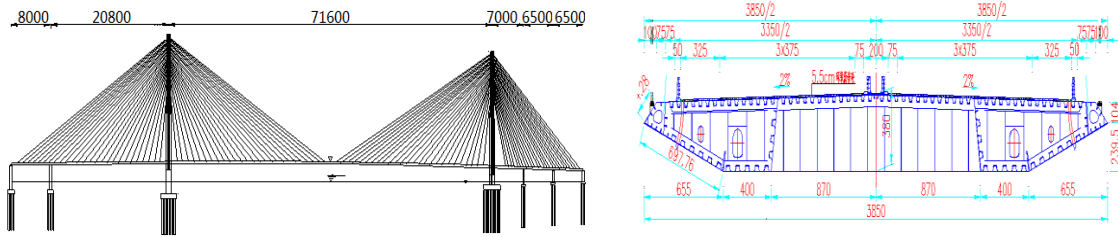


Fig. 6 The Jinyu Highway Bridge (cm)

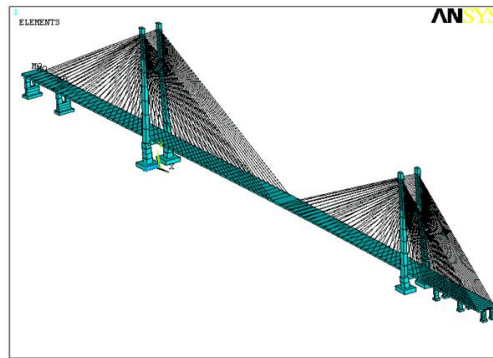


Fig. 7 The full bridge model

4.2 Traffic flow simulation considering the influence of the next-nearest neighbor vehicles

Using Eqs. (23) and (24) that consider the influence of the next-nearest neighbor vehicles, the two-lane cellular automata model with the influence of the next-nearest neighbor vehicles was established for the Jinyu highway bridge. The similar bridge has been selected as the prototype bridge in several previous studies (e.g., Chen *et al.* 2007). The approaching roadway at each end of the bridge is assumed to be 1005 m, \dot{x}_{\max} can be computed as 5 (cell/s), and the speed limit of the highway system is 135(km/h). The sensitivity coefficients of the nearest neighbor and next nearest neighbor vehicles are $\lambda_1=0.2$ and $\lambda_2 =0.05$ (Kong *et al.* 2006). The traffic flow simulation results with the CA model usually become stable after a continuous simulation with a period equal to 10 times the cell numbers of the traffic simulating system (Nagel and Schreckenberg 1992, Chen *et al.* 2007). For the comparison purpose, two different vehicle occupancies ρ are considered (Chen and Wu 2011): median traffic ($\rho=0.15$) and busy traffic flow ($\rho=0.3$). It can be found from Fig.8 that the x-axis and y-axis represent the coordinates in both the spatial and time domains, respectively, and each dot in the figures represents a vehicle. With the increase of the traffic occupancy, local congestions may be formed at some locations as indicated by the black belts in Fig. 8.

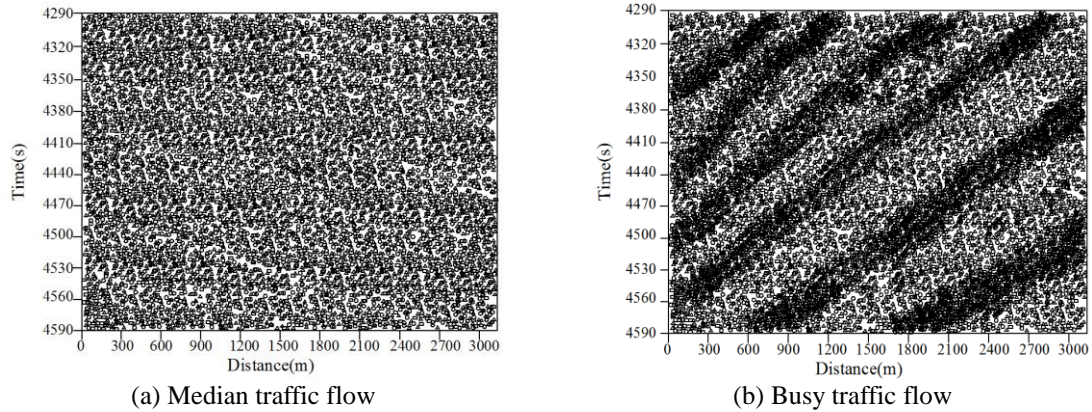


Fig. 8 Traffic simulation with different vehicle occupancies

4.3 Comparison of the effects with and without considering the next-nearest neighbor vehicles in traffic flow

Some typical factors including the traffic flow occupancies (smooth traffic $\rho=0.07$ and median traffic $\rho=0.15$) and wind speeds (weak wind speed $U=2.7$ m/s and moderate wind speed $U=17.6$ m/s) were used in the studies (e.g., Chen and Wu 2011). In the following sections, the same factors were used to study the bridge responses.

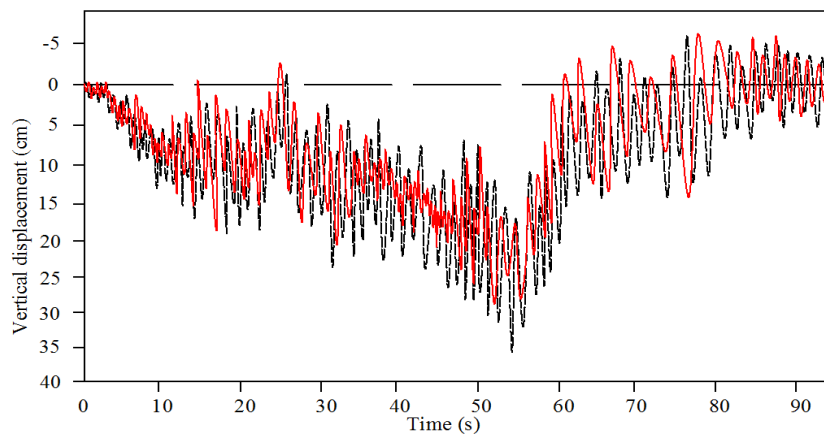
As discussed earlier, some simplified traffic flow models did not take into account the effects of the next-nearest neighbor vehicles, thus, the effects on the bridge responses were studied. The time histories of the responses at the mid-span of the bridge under two typical traffic flows with and without considering the next-nearest neighbor vehicles under moderate wind speed ($U=17.6$ m/s) are presented in Fig. 9. It is found that the maximal displacement at the mid-span for the traffic flow without considering the next-nearest neighbor vehicles are greater than that for with the considering the next-nearest neighbor vehicles. For example, the maximal vertical displacements of bridge are equal to 28.6 cm and 35.7 cm corresponding to with and without considering the next-nearest neighbor vehicles, respectively. This phenomenon could be explained that the characteristics of the traffic, such as speed of vehicles and distance of each vehicle, can be changed due to considering the effects of the next-nearest neighbor vehicles.

4.4 Comparison of the bridge responses with different traffic flow occupancies

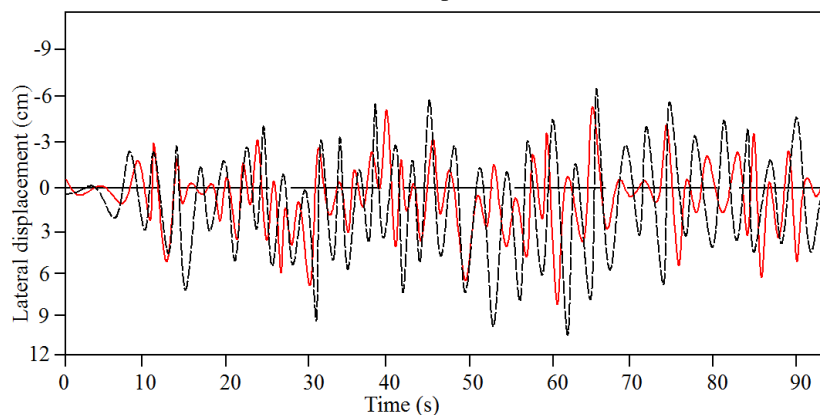
The time histories of the vertical and lateral responses at the mid-span of the bridge under two different traffic flow occupancies with moderate wind speed ($U=17.6$ m/s) are presented in Fig. 10. It is found that the displacements at the mid-span increases generally with the vehicle occupancy increases. The vehicle occupancies play a significant role on the bridge displacements. For example, the maximal vertical displacements of bridge increases from 28.6 cm to 42.3 cm when the vehicle occupancy increases from smooth traffic ($\rho=0.07$) to median traffic ($\rho=0.15$).

4.5 Comparison of the bridge responses under traffic flow with different wind speeds

The time histories of the responses at the mid-span of the bridge under two typical wind speeds (weak wind speed $U=2.7$ m/s and moderate wind speed $U=17.6$ m/s) with the traffic flow occupancy $\rho=0.07$ are presented in Fig.11. It is found that the displacements and accelerations at the mid-span increase generally with the increase of wind speeds, as expected. The wind speed plays a significant role on the bridge displacements, especially for the lateral displacement. For example, when the wind speed increases from 2.7 m/s to 17.6 m/s, the maximal vertical displacements increase from 21.3 cm to 28.6 cm, and the maximal lateral displacements increase from 3.1 cm to 8.7 cm. The effects of wind speed on the lateral displacements are more than those of wind speed on the vertical displacements.

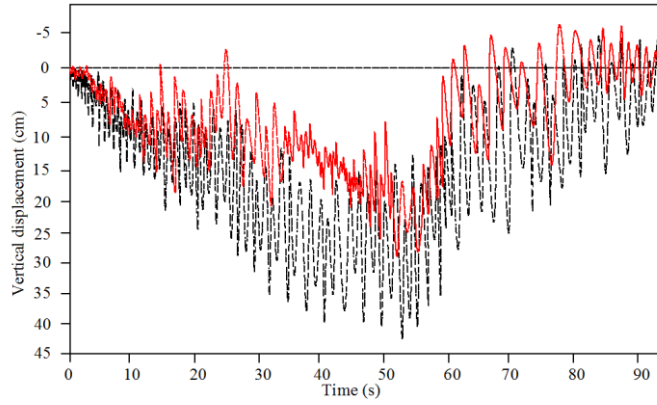


(a) Vertical displacement

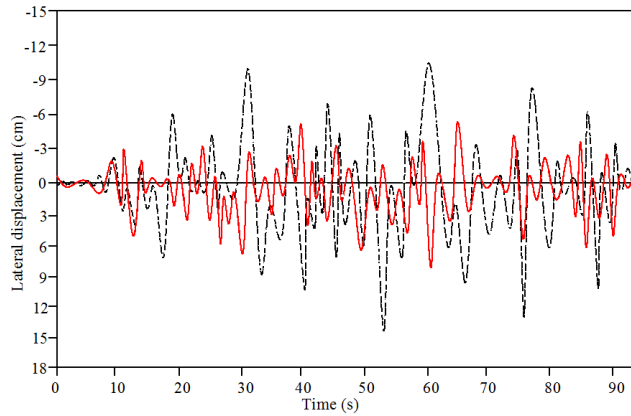


(b) Lateral displacement

Fig. 9 The bridge responses under two different traffic flow occupancies (considering next-nearest neighbor vehicle —; without considering next-nearest neighbor vehicles — —)

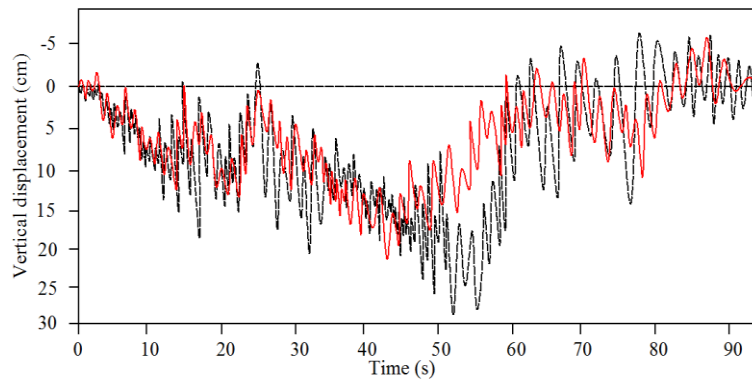


(a) Vertical displacement



(b) Lateral displacement

Fig. 10 The bridge responses under two different traffic flow occupancies (smooth traffic $\rho=0.07$ —; median traffic $\rho=0.15$ - - -)



(a) Vertical displacement

Continued-

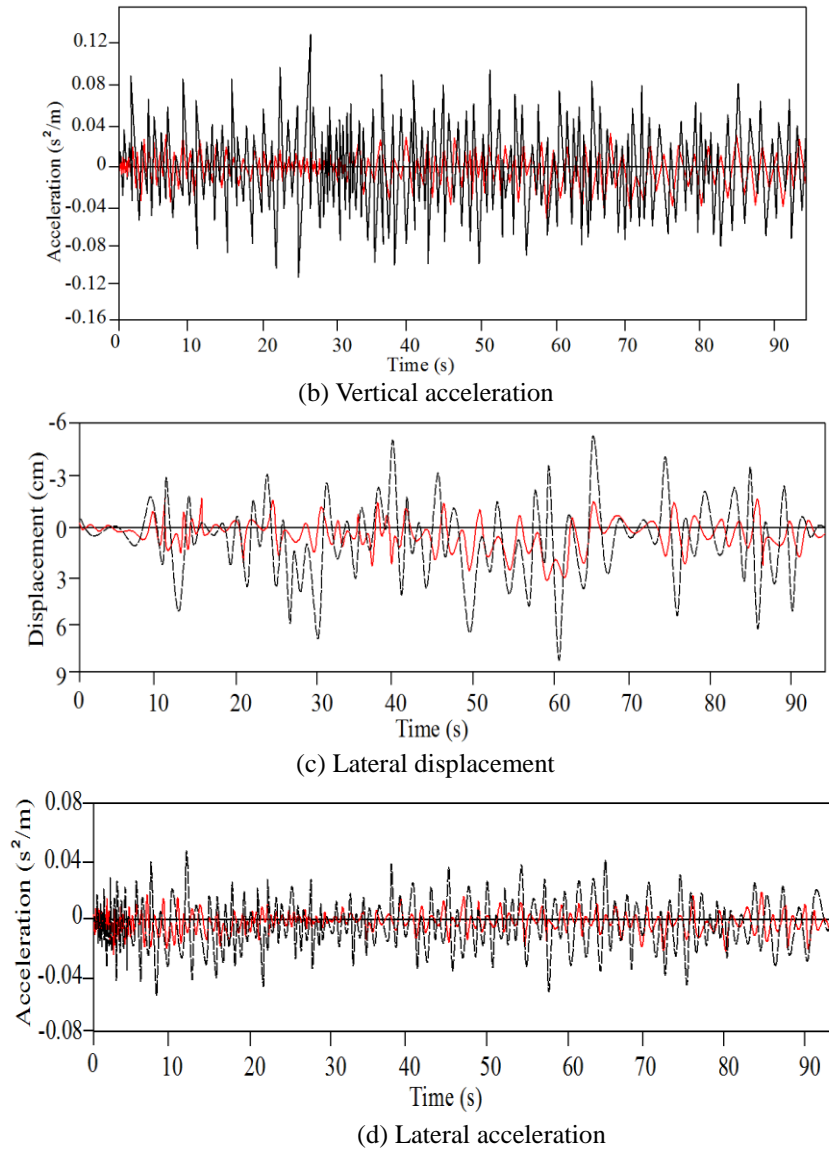
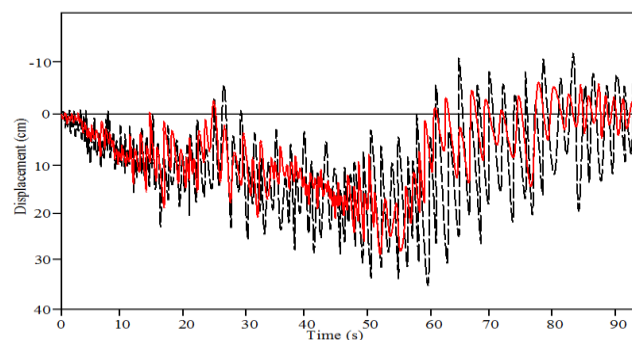


Fig. 11 The responses at the midpoint of the bridge under two different wind speed (weak wind speed —; moderate wind speed — —)

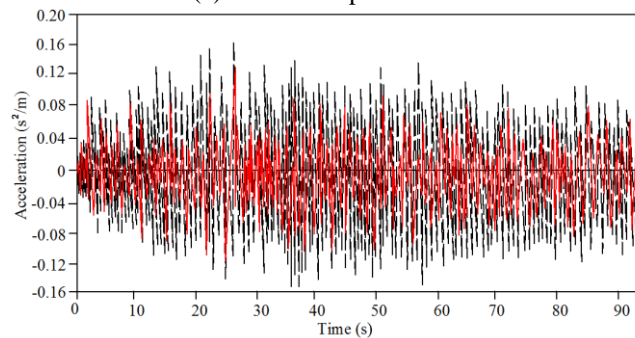
4.6 Comparison of the bridge responses in wind environment under stochastic traffic loads with roughness progressive deterioration

It can be obtained from Table 1 that the bridge surface roughness would be deterioration as the year increases due to loads or corrosions. For example, in the first 13 years for the slow lane, the classification of bridge surface would be very good classification for 8th years to the poor

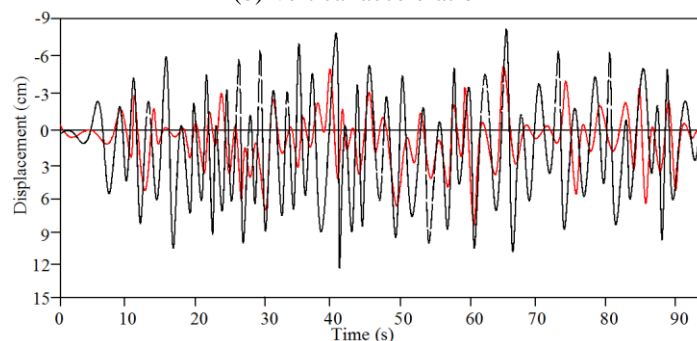
classification for 13th years. Thus, this section, the two special times of 8th and 13th years were used to study the responses at the mid-span of the bridge. Fig. 12 shows the bridge responses in moderate wind speed under stochastic traffic load with roughness progressive deterioration. It is found that the displacements and accelerations at the mid-span increase generally with the year increases due to the bridge roughness progressive deterioration. Thus, the bridge roughness plays a significant role on the bridge displacement and acceleration, as expected. For example, the bridge vertical displacement increases from 28.6cm to 34.8 cm when the year increases from the 8th to 13th year when the other conditions are the same. Thus, regular maintenance of the bridge surface is a very effective way of reducing ride comfort for the long span bridge.



(a) Vertical displacement



(b) Vertical acceleration



(c) Lateral displacement

Continued-

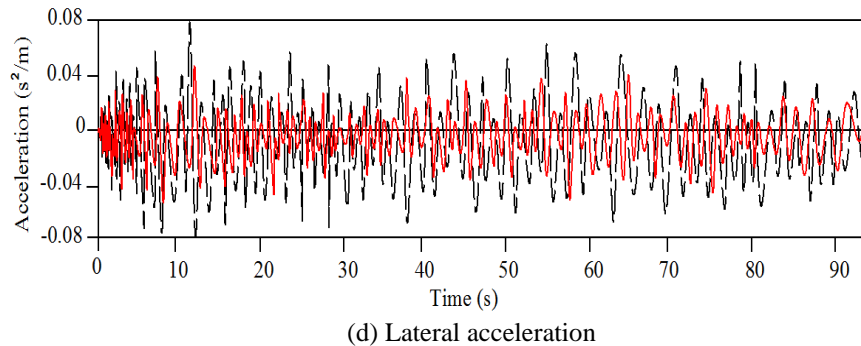


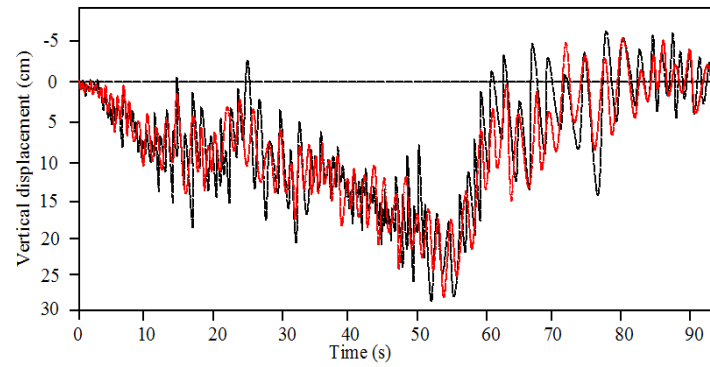
Fig. 12 The responses of the bridge with roughness progressive deterioration (8th year —; 13th year - - -)

4.7 Comparison of the bridge responses in wind environment under stochastic traffic load with different vehicle models

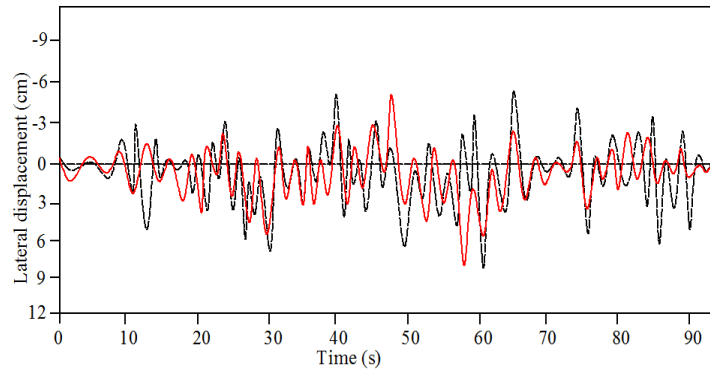
As discussed earlier, some simplified vehicle models were used usually to study the bridge responses for the simplification by ignoring the seat itself vibration (Xu and Guo 2004, Yin *et al.* 2011), and a verification of this simplification needs to be performed before using it with confidence. Thus, in this section, a three dimensional vehicle model including three-dimensional non-linear suspension seat model, as developed earlier, was used to study the bridge responses. The time histories of the dynamic bridge responses under two different (simplified vehicle model and present vehicle model) with the traffic flow occupancy $\rho=0.07$ are presented in Fig. 13. It is found that the general effect tendency of the two different vehicle models on the displacements at the mid-span are similar and the maximal displacements are almost equal to each other, thus, those effects on the dynamic responses of bridge may be neglectable, though some values at the same time are different between the two simulations.

4.8 Comparison of the ride comfort in wind environment under stochastic traffic load with different vehicle models

As discussed earlier, some simplified vehicle models were used to study the ride comfort for the simplification by ignoring the seat itself vibration (Xu and Guo 2004, Yin *et al.* 2011), and a verification of this simplification needs to be performed before using it with confidence. Thus, in this section, a three dimensional vehicle model including three-dimensional non-linear suspension seat model, as developed earlier, was used to study the ride comfort. The total values of the weighted RMS accelerations a_w of the occupant mass are calculated directly with the different vehicle occupancies, wind speeds, and year increases. The corresponding ride comfort is given in Tables 6-8. It can be seen that the vertical, lateral, and longitudinal vibrations of the detailed driver seat model can significantly affect the drive comforts with the factors including the different vehicle occupancies, wind speeds and year increases. The simplified vehicle model, if used to study the ride comfort, may easily result in imprecise conclusions. For example, the classification of ride comfort changes from not uncomfortable to a little uncomfortable if the vehicle of the present model is changed to the simplified model when the vehicle occupancy $\rho=0.07$.



(a) Vertical displacement



(b) Lateral displacement

Fig. 13 Bridge responses under stochastic traffic load with different vehicle models (Simplified model —; Present model - - -)

Table 6 Ride comfort with two vehicle occupancies (m/s^2)

Vehicle occupancies		a_{sux}	a_{suy}	a_{suz}	a_{su}	Comfort or Discomfort
$\rho=0.07$	Present model	0.06	0.12	0.23	0.30	Not uncomfortable
	Simplified model	0.14	0.16	0.29	0.41	A little uncomfortable
$\rho=0.15$	Present model	0.12	0.19	0.32	0.45	Fairly uncomfortable
	Simplified model	0.17	0.28	0.35	0.58	Fairly uncomfortable

Table 7 Ride comfort with two wind speeds (m/s^2)

Wind speeds		a_{sux}	a_{suy}	a_{suz}	a_{su}	Comfort or Discomfort
U=2.7 m/s	Present model	0.02	0.09	0.12	0.18	Not uncomfortable
	Simplified model	0.05	0.10	0.15	0.22	Not uncomfortable
U=17.6 m/s	Present model	0.06	0.10	0.23	0.30	Not uncomfortable
	Simplified model	0.14	0.16	0.29	0.41	A little uncomfortable

Table 8 Ride comfort with year increases (m/s^2)

Year increases		a_{sux}	a_{suy}	a_{suz}	a_{su}	Comfort or Discomfort
8years	Present model	0.06	0.12	0.23	0.30	Not uncomfortable
	Simplified model	0.14	0.16	0.29	0.41	A little uncomfortable
13years	Present model	0.13	0.22	0.28	0.45	A little uncomfortable
	Simplified model	0.18	0.27	0.36	0.57	Fairly uncomfortable

5. Conclusions

This paper presents a new methodology to study the ride comfort of a long-span bridge-traffic-wind coupled vibration system considering stochastic characteristics of traffic flow and bridge surface conditions. A three-dimensional vehicle model including a three-dimensional non-linear suspension seat model is presented to study the ride comfort. An improved CA model that considers the influence of the next-nearest neighbor vehicles and a progressive deterioration model for bridge-roughness are introduced. The bridge-traffic-wind coupled equations are established by combining the equations of motion of both the bridge and vehicles using the displacement relationship and interaction force relationship at the patch contact. The following conclusions can be drawn:

- (1) An improved CA model that considers the influence of the next-nearest neighbor vehicles can be introduced to study the vibration of bridge-traffic-wind coupled systems, the maximal bridge displacements for the traffic flow without considering the next-nearest neighbor vehicles are greater than maximal bridge displacements for with the considering the next-nearest neighbor vehicles.
- (2) The vehicle occupancy and wind speed play significant roles on the bridge displacements. The maximal vertical displacement of bridge increases from 28.6 cm to 42.3 cm when the vehicle occupancy increases from 0.07 to 0.15.
- (3) The progressive deterioration model for bridge-roughness plays a significant role on the bridge responses. The bridge maximal vertical displacement increases from 28.6 cm to 34.8 cm when the year increases from 8th to 13th year. Thus, regular maintenance of the bridge surface is a very effective way of reducing ride comfort for the long span bridge.
- (4) The effect of driver seat model on the dynamic responses of bridge may be neglectable, but the vertical, lateral, and longitudinal vibrations of the driver seat model can significantly affect the drive comforts. Thus, the present vehicle model can be used to study the ride comfort with good accuracy.

Acknowledgments

The authors gratefully acknowledge the financial support provided by the National Basic Research Program of China (973 Program) (Project No. 2015CB057702), and the Natural Science Foundation China (Project No.51108045; 51178066), and the Fund of Hunan Provincial Youth Talent (Project No. 2015RS4052).

References

- Baker, C. J. (1991), "Ground vehicles in high cross winds. Part I: Unsteady aerodynamic forces", *J. Fluid. Struct.*, **5**, 91-111.
- Bouazara, M., Richard, M.J. and Rakheja, S. (2006), "Safety and comfort analysis of a 3-D vehicle model with optimal non-linear active seat suspension", *J. Terramech.*, **43**, 97-118.
- Cai, C.S., Hu, J., Chen, S., Han, Y., Zhang, W. and Kong, X. (2015), "A coupled wind-vehicle-bridge system and its applications: a review", *Wind Struct.*, **20**(2), 117-142.
- Chen, S.R. and Cai, C.S. (2004), "Accident assessment of vehicles on long-span bridges in windy environments", *J. Wind Eng. Ind. Aerod.*, **92**(12), 991-1024.
- Chen, Y.B. and Feng, M.Q. (2006), "Modeling of traffic excitation for system identification of bridge structures", *Comput-Aided Civ. Infrastruct Eng*, **21**, 57-66.
- Chen, S.R. and Cai, C.S. (2007), "Equivalent wheel load approach for slender cable-stayed bridge fatigue assessment under traffic and wind: feasibility study", *J. Bridge Eng.*, **12**(6), 755-764.
- Chen, S.R. and Wu, J. (2010), "Dynamic performance simulation of long-span bridge under combined loads of stochastic traffic and wind", *J. Bridge Eng.*, **15**(3), 219-230.
- Chen, S.R. and Wu, J. (2011), "Modeling stochastic live load for long-span bridge based on microscopic traffic flow simulation", *Comput. Struct.*, **89**, 813-824.
- Clough, R.W. and Penzien, J. (1993), "Dynamics of structures" [M], New York, McGraw-Hill Inc.
- Deng, L. and Cai, C.S. (2010), "Bridge model updating using response surface method and genetic algorithm", *J. Bridge Eng.*, **5**(15), 553-564.
- Fujii, S. and Yoshimoto, K. (1975), "An analysis of the lateral hunting motion of a two-axle railway wagon by digital simulation (1st report, the outline of the mathematical model)", *Bull. JSME*, **18**(122), 813-818.
- Fujii, S., Yoshimoto, K. and Kobayashi, F. (1975), "An analysis of the lateral hunting motion of a two-axle railway wagon by digital simulation (2nd report, the outline of the mathematical model)", *Bull. JSME*, **18**(125), 1246-1251.
- Gim, G. and Nikravesh, P.E. (1990), "Analytical model of pneumatic types for vehicle dynamic simulations Part I. Pure slips", *Int. J. Vehicle Des.*, **11**(5), 589-618.
- Guo, W.H. and Xu, Y.L. (2001), "Fully computerized approach to study cable-stayed bridge vehicle interaction", *J. Sound Vib.*, **248**(4), 745-761.
- Han, W., Ma, L., Cai, C.S., Chen, S. and Wu, J. (2015), "Nonlinear dynamic performance of long-span cable-stayed bridge under traffic and wind", *Wind Struct.*, **20**(2), 249-274.
- ISO. (1995), "Mechanical vibration-road surface profiles-reporting of measured data", ISO 8068: (E), Geneva.
- ISO. (1997), "Mechanical vibration and shock - Evaluation of human exposure to whole body vibration-Part1: General requirements", ISO 2631-1:1997E, Geneva.
- Park J.H., Huynh T.C., Lee K.S. and Kim J.T. (2016), "Wind and traffic-induced variation of dynamic characteristics of a cable-stayed bridge-benchmark study", *Smart Struct. Syst.*, **17**(3), 491-522.
- Kong, X., Gao, Z. and Li, K. (2006), "A two lane cellular automata model with influence of next nearest neighbor vehicle", *Commun. Theor. Phys.*, **45**(4), 657-662.
- Nagel, K. and Schreckenberg, M. (1992), "A cellular automaton model for freeway traffic", *J. Phys. (France)*, **2**(12), 2221-2229.
- Zhang, W. and Cai, C.S. (2012), "Fatigue reliability assessment for existing bridges considering vehicle speed and road surface conditions", *J. Bridge Eng.*, **17**(3), 443-453.
- Xu, Y.L. and Guo, W.H. (2004), "Effects of bridge motion and crosswind on ride comfort of road vehicles", *J. Wind Eng. Ind. Aerod.*, **92**, 641-662.
- Yin, X.F., Fang, Z. and Cai, C.S. (2011), "Lateral vibration of high-pier bridges under moving vehicular loads", *J. Bridge Eng.*, **16**(3), 400-412.
- Yu, L. and Chan, T.H. (2007), "Recent research on identification of moving loads on bridges", *J. Sound Vib.*, **305**(1-2), 3-21.

CC